

# Mesoporous Coatings with Simultaneous Light-Triggered Transition of Water Imbibition and Droplet Coalescence

Adnan Khalil, Peyman Rostami, Günter K. Auernhammer, and Annette Andrieu-Brunsen\*

A systematic study of gating water infiltration and condensation into ceramic nanopores by carefully adjusting the wetting properties of mesoporous films using photoactive spiropyran is presented. Contact angle measurements from the side reveal significant changes in wettability after irradiation due to spiropyran/merocyanine-isomerization, which induce a wetting transition from dry to wet pores. The change in wettability allows the control of water imbibition in the nanopores and is reflected by the formation of an imbibition ring around a droplet. Furthermore, the photoresponsive wettability is able to overcome pinning effects and cause a movement of a droplet contact line, facilitating droplet coalescence, as recorded by high-speed imaging. The absorbed light not only effectuates droplet merging but also causes flows inside the drop due to heat absorption by the spiropyran, which results in gradients in the surface tension. IR imaging and particle tracking is used to investigate the heat absorption and temperature-induced flows, respectively. These flows can be used to manipulate, for example, molecular movement inside water and deposition inside solid mesoporous materials and are therefore of great importance for nanofluidic devices as well as for future water management concepts, which include filtering by imbibition and collection by droplet coalescence.

management concepts: first, controlled and gated water imbibition and condensation into nanoscale pores; second, drop coalescence. To study both, ceramic mesoporous thin films are interesting model systems, and their manufacture<sup>[4]</sup> and functionalization<sup>[5]</sup> have been examined deeply in the last 25 years.<sup>[6]</sup> Water manipulation on and in such films or separation layers has been intensively investigated more recently.<sup>[7]</sup> However, in comparison to planar and structured surfaces, the possibilities for the control of wettability and consequently of water imbibition, condensation, and drop coalescence in mesopores have been much less investigated and are less well understood. In recent years, the main interest with respect to the wettability of surfaces has been the development of superhydrophobic, superamphiphobic, or nonicing surfaces.<sup>[8]</sup> The approaches used are often inspired by naturally occurring surfaces, such as the lotus leaf, pitcher plant, or fog basking beetles, and are always based on a

## 1. Introduction

Wettability in nanoscale space is of great significance for understanding many increasingly relevant problems, such as water or liquid processing,<sup>[1]</sup> catalysis,<sup>[2]</sup> and energy storage and conversion.<sup>[3]</sup> In this context, two phenomena are of significant importance, especially regarding liquid processing and future water


combination of surface structure on the micro- and nanometer scale with correspondingly hydrophobic surface chemistry,<sup>[8b,9]</sup> or with hydrophobic lubricants enclosed in a porous structure.<sup>[10]</sup> One challenge is to achieve a sufficiently large change in wettability upon switching of responsive functional groups.<sup>[9b]</sup> By altering the contact angle of drops on the surface as well as the contact line, which is essential for applications such as drop merging, for example, this change in wettability is explored to be used in the context of water generation from humidity.<sup>[11]</sup> One of the common applications is self-removal substrates, which collect condensed droplets and remove them from structured substrates.<sup>[12]</sup> In most cases, macro-<sup>[13]</sup> and microstructured<sup>[14]</sup> surfaces are used to enhance the self-cleaning processes. During self-cleaning or fog-harvesting processes, drop coalescence on structured surfaces is one of the rate-controlling processes.<sup>[15]</sup> Light-driven movement of liquid drops also offers to control droplet-based processes.<sup>[16]</sup> Using light-driven drop coalescence would allow the use of contact-free drop coalescence in processes such as water collection or fundamental investigations such as undisturbed (photoinduced) drop coalescence.

Wettability can be made stimuli-responsive by utilizing functional groups with switchable polarity or by designing the micro- or nanoscale structure to change upon stimuli impact.<sup>[17]</sup> A frequently used stimulus is light, as it can be adjusted externally and gradually. A highly interesting molecule which is responsive to light is, for example, the spiropyran. As nicely reviewed by Klajn et al., the spiropyran was subject of many

A. Khalil, Prof. A. Andrieu-Brunsen  
Technische Universität Darmstadt  
Ernst-Berl-Institut für technische und makromolekulare Chemie  
64289 Darmstadt, Germany  
E-mail: andrieu-brunsen@smartmem.tu-darmstadt.de

P. Rostami, Dr. G. K. Auernhammer  
Leibniz-Institut für Polymerforschung Dresden e.V.  
Institut für Physikalische Chemie und Physik der Polymere  
01069 Dresden, Germany

P. Rostami, Dr. G. K. Auernhammer  
Max-Planck-Institut für Polymerforschung  
Physik der Grenzflächen  
55128 Mainz, Germany

 The ORCID identification number(s) for the author(s) of this article can be found under <https://doi.org/10.1002/admi.202100252>.

© 2021 The Authors. Advanced Materials Interfaces published by Wiley-VCH GmbH. This is an open access article under the terms of the Creative Commons Attribution-NonCommercial License, which permits use, distribution and reproduction in any medium, provided the original work is properly cited and is not used for commercial purposes.

DOI: 10.1002/admi.202100252

studies to design dynamic materials.<sup>[18]</sup> Spiropyran can be used as molecular switches that undergoes a photoisomerization to a merocyanine in response to different orthogonal stimuli such as light, temperature, mechanical stress, redox potential, or metal ions. During this isomerization, the properties of the molecule change drastically. The charge separation in the merocyanine effectuates a large electrical dipole ( $\approx 14\text{--}18$  D) moment which is significantly higher than for the spiropyran ( $\approx 4\text{--}6$  D).<sup>[19]</sup> This increase in dipole moment and therefore surface polarity manifests itself in the change of wetting properties. On flat, non-structured surfaces, the photoisomerization of the molecules causes only a minor change of  $\approx 10^\circ$  in the contact angle.<sup>[9c,18]</sup> When attached to a structured surface, photoisomerization potentially has a more severe effect on the wetting properties of the material due to the possibility of wetting transitions. For example, Dattilo et al. described a slight increase in contact angle change when spiropyran is irradiated while attached to a porous surface instead of a flat surface.<sup>[20]</sup> Rosario et al. found a change of  $22^\circ$  in wetting properties when spiropyran was attached to rougher (nano- or microscale) silicon nanowires.<sup>[21]</sup> Only with the use of additional metal(II) ions for enhancing the merocyanine form, larger contact angle differences of  $32\text{--}35^\circ$  were achieved.<sup>[20,22]</sup> A higher change of contact angle caused by pure illumination could be achieved by neither Dattilo et al. nor Rosario et al. because the photoisomerization was not coupled to wetting-transition. In this context, Groten et al. provided insights into the interplay between roughness (black silicon) and photochemical switching of an azobenzene containing polymer monolayer by carefully tuning the surface polarity close to wetting transitions.<sup>[9c]</sup> By coupling the photoprocess to a wetting transition of the substrate, extremely large changes in contact angle could be achieved on structured surfaces. Nevertheless, it has not yet been investigated how such concepts can be transferred to mesoporous thin films with pores smaller than 20 nm and thicknesses below 1  $\mu\text{m}$  and how water infiltration or drop coalescence can be gated using light as the stimulus to change the wettability of a mesoporous layer. In a theoretical study, an abrupt transition between fully wetted and dry surfaces, which is above Wenzel's contact angle, has been demonstrated for mesoscale structured surfaces.<sup>[23]</sup> In addition, these nanoscale pores in the format of nanoscale thin coatings are complex, as evaporation and condensation affect wetting behavior and must be considered.<sup>[7c]</sup> Furthermore, when light is used as a trigger, heat absorption due to irradiation must be regarded, as this can alter the temperature of the substrate, leading to Bénard–Marangoni convection.<sup>[24]</sup> Formed convection cells can be used to manipulate the flow inside the droplet and induce a specified deposition of molecules on a surface.<sup>[25]</sup>

In this study, we coupled a spiropyran-photoswitch to a wetting transition for ceramic mesoporous thin films. Therefore, the contact angle prior to the photoisomerization must not be higher than  $\approx 10^\circ$  above the threshold contact angle that defines the wetting transition, as this is the change in contact angle that spiropyran can achieve on a plane surfaces. The functionalization strategy was kept as simple as possible, and the grafting conditions for a monolayer layer were optimized. A wetting transition from water exclusion to water infiltration could be induced, detected by an abrupt increase in the light-induced contact angle change, as compared to the same switching more

far away from a transition, accompanied by water imbibition. This water imbibition into the mesoporous coating is visible by a ring-shaped imbibed zone around a deposited water droplet, which was monitored using a top view camera. A contact angle decrease of  $\approx 30^\circ$  was observed upon photoinduced water imbibition. This shows that small changes in surface energy near a wetting transition have an increased effect on the wetting properties, even for substrate-supported mesoporous thin films. In addition, this wetting transition as a tool for light-induced droplet manipulation and coalescence is discussed. We expect these results to impact mesoporous thin film applications, for example, in electronics or optics, as well as open new fields, for example, regarding separation or water collection by condensation and drop coalescence from humidity.

## 2. Results and Discussion

### 2.1. Spiropyran Modification of Mesopores

#### 2.1.1. Light-Gated Wettability and Water Imbibition into Mesopores

Mesoporous silica thin films were prepared via sol-gel synthesis and evaporation-induced self-assembly (EISA) using a sol containing tetraethyl orthosilicate (TEOS) as the silica precursor and the block-copolymer template Pluronic F127. In agreement with previous studies,<sup>[4,26]</sup>  $\approx 170$  nm thick mesoporous silica thin films with a pore diameter of  $\approx 6\text{--}8$  nm and a neck diameter of  $\approx 2\text{--}3$  nm were obtained, as verified by transmission electron microscopy (TEM) imaging (**Figure 1a**). As schematically described in the Experimental Section in Schemes 2 and 3, the surface-active hydroxyl groups of the mesoporous silica materials were used for amine and subsequent spiropyran grafting. In general, different amines, such as 3-aminopropyltriethoxy silane (APTES), 3-aminopropyltrimethylmethoxy silane (APDMMS), or 3-aminopropyl dimethylethoxy silane (APDMES), were used for modification. After the attachment of spiropyran and exposure to UV light (inducing isomerization to the merocyanine form), all samples showed a strong violet coloration (independent of the amine used), as shown for APDMES in **Figure 1a**, which can also be verified by UV–vis spectroscopy (**Figure 1b**). Before irradiation with UV light (see Experimental Section for details), the spiropyran-modified samples exhibited a maximum absorption at  $\approx 340$  nm in the UV–vis spectrum as well as a smaller absorption maximum at  $\approx 560$  nm (black curve) corresponding to the merocyanine form,<sup>[18]</sup> which drastically increased after exposure to UV light (magenta curve).

The sample coloration and the corresponding spectra showed that the mesopores were clearly accessible for modification. As a reference experiment, a nonporous dense silica film and mesoporous silica film were modified under identical conditions, and a UV–vis spectrum was recorded from both samples. Compared to the mesoporous film, the dense silica film showed no detectable absorption maxima, indicating that the spiropyran amounts of a single outer layer were not sufficient to cause visible coloration or measurable absorption (see **Figure S2**, Supporting Information). Furthermore, the coloration proved that photoisomerization still takes place in nanoconfinement. Krohm et al. showed similar results by attaching

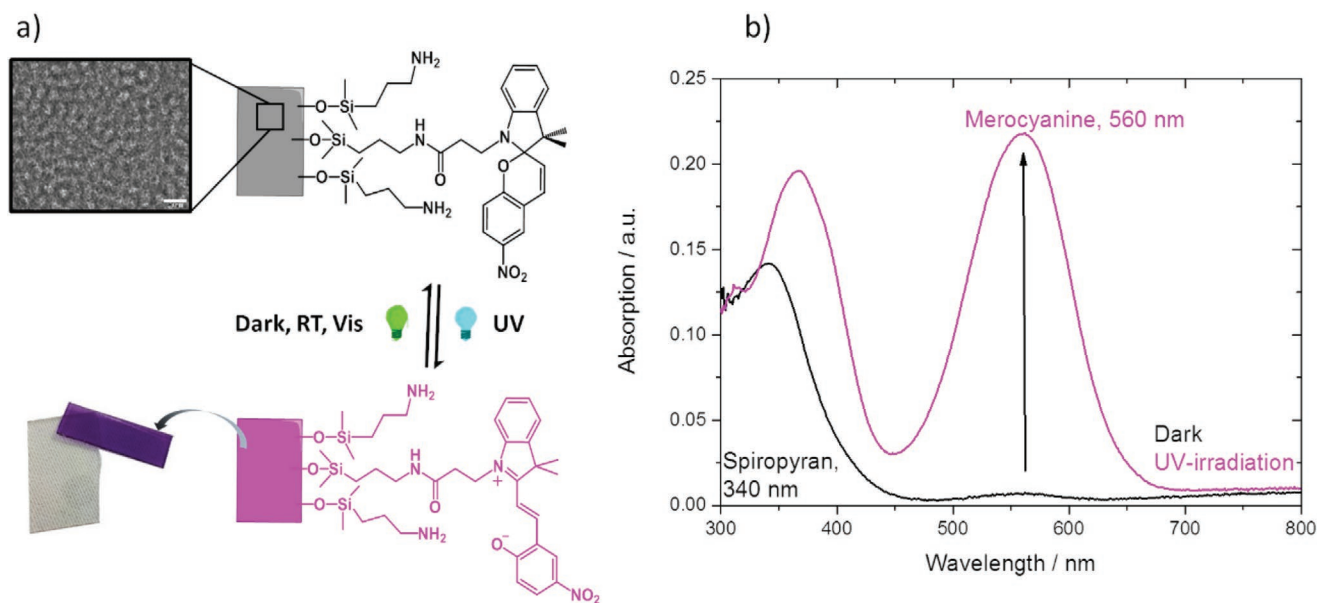


**Figure 1.** a) Photoisomerization of spiropyran and merocyanine while attached to a mesoporous silica thin film as indicated by a TEM image (scale bar = 20 nm). When deposited on a glass substrate, the color change (colorless to violet) of the mesoporous silica thin film upon photoisomerization became obvious at room temperature (RT). b) This can also be measured by UV-vis spectroscopy, as shown in the spectrum. Before UV irradiation (black), only one pronounced maximum was observed at 340 nm (spiropyran). After UV irradiation (magenta, irradiation time = 30 s), a second maximum emerged at 560 nm (merocyanine).

spiropyran and spirooxazines in the form of polynorbornene oligomers to mesopores.<sup>[27]</sup> A surface and confinement effect in the kinetics of the photoconversion was shown. This became particularly visible for the samples discussed here, when looking at the thermal relaxation of surface bound merocyanine isomers compared to the dissolved species. Increased stabilization of the polar isomer by the hydrophilic silica matrix led to a significant increase in thermal relaxation times (see Figure S3, Supporting Information).<sup>[28]</sup> When dissolved in dimethylformamide, the merocyanine relaxed almost completely to the spiropyran isomer within 15 min. However, when attached to silica mesopores, the thermal relaxation from merocyanine to spiropyran was not completed even after 60 min. Approximately five percent of the maximum achieved amount of merocyanine did not relax.

The effect of the spatial confinement and silica surface on the spiropyran–merocyanine equilibrium must also be considered for the investigation of the wetting properties. In this context, the first step of amine coupling should be performed with special care. Although chemically simple, this first step strongly influences subsequent spiropyran binding. It is known from the literature that an elevated binding temperature has a positive effect on the hydrolytic stability of the bond,<sup>[29]</sup> which is why all aminosilanes in this work were grafted in dry toluene at 80 °C. Furthermore, APDMES was mainly used as an anchor group to limit the possible orientations and branching of the aminosilanes at the surface, since these factors are also known to affect the wettability.<sup>[29a]</sup> As recently shown, an organic monofunctional anchor group does not affect the root mean square roughness ( $S_q$ ) of mesoporous silica thin films drastically.<sup>[26b]</sup> Prior to functionalization, the  $S_q$  was rather low (0.36 nm) and remained on the same scale afterwards (0.39 nm).

Varying the concentration (c) of the aminosilane in the reaction solution between 0.005 and 0.05 wt% under otherwise constant binding conditions (toluene, 80 °C, 2 h) resulted in a similar deposited contact angle (CA) of 65° and refractive index (RI) of 1.32 after 2 h (see Figure S4, Supporting Information). However, increasing the aminosilane concentration to 0.065 wt% resulted in an unusually high CA of >100°, regardless of which amine was used (APDMES, APDMMS, APTES, see Figure S5a, Supporting Information). Scanning electron microscope images after APTES binding from a 0.065 wt% solution revealed agglomerate formation and thus the generation of a rougher structure, as agglomerates of several hundred nm in size were clearly visible on the mesoporous film (see Figure S5b, Supporting Information).

Since variation in the concentration was not suitable to adjust the initial wettability, a fixed APDMES concentration of 0.01 wt% in toluene was initially chosen, and the binding time of the functionalization was varied (Figure 2a).

As shown in Figure 2b, by adjusting the reaction time of APDMES, the CA of the materials can be adjusted between 50° and 80°. While the initial CA of an unfunctionalized mesoporous silica thin film before APDMES bonding was ≈20°,<sup>[26b]</sup> it reached ≈70–80° after 2 h of reaction time. As the reaction time increased, the proportion of organic molecules on the inorganic silica surface increased, which reduced its hydrophilicity. However, ellipsometry measurements showed that the RI and thus the pore filling (≈43%) did not significantly change after different reaction times (Figure 2c, green). This indicates that the different reaction times probably have a particular effect on the number of amino anchors on the outer surface of the mesoporous films, which directly influences the macroscopic wetting properties detected by the CA (Figure 2b).

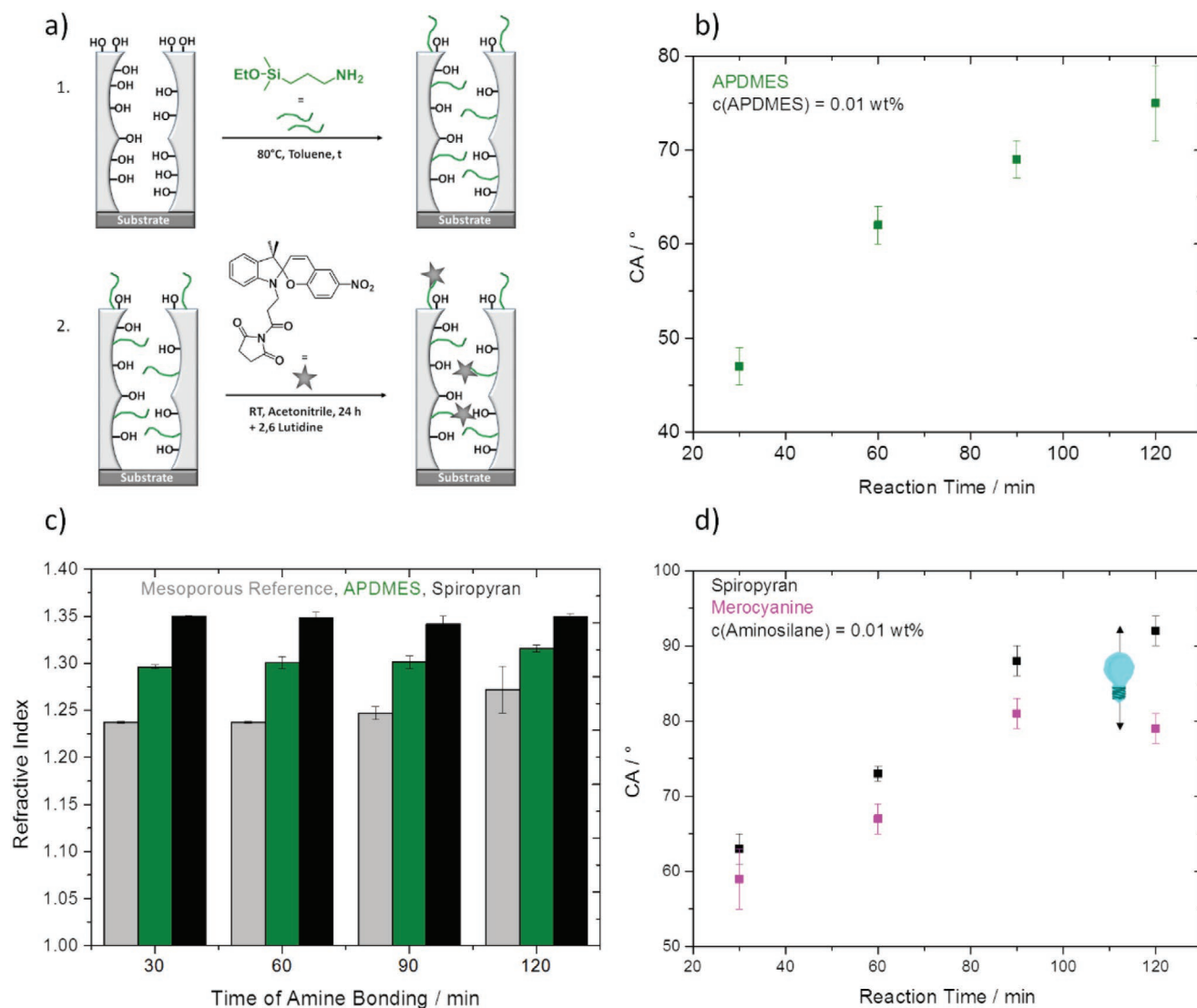


**Figure 2.** a) Surface functionalization of mesoporous silica thin films with APDMES for different intervals of time ( $t$ ) at  $80^\circ\text{C}$  (1) and spiropyran at room temperature (RT) for 24 h (2). b) CA of mesoporous silica thin films after APDMES bonding ( $c = 0.01$  wt%) for different time intervals. c) Refractive index of mesoporous silica thin films before (gray) and after different times of amine functionalization (green) with subsequent spiropyran esterification (black). d) CA of mesoporous silica thin films after spiropyran modification (black) with subsequent UV irradiation (magenta, irradiation time = 30 s) as a function of prior APDMES bonding time.

The same trends in CA and RI after APDMES bonding continued after spiropyran grafting. RI and therefore pore filling increased ( $\approx 61\%$ ), but the RI increase upon spiropyran binding did not show differences in dependence of the APDMES reaction time (Figure 2c, black), while CA values showed an increasing trend with increasing reaction time and even reached values above  $90^\circ$ , which implies water exclusion (Figure 2d, black). After exposure to UV light and thus the formation of merocyanine, the spiropyran-modified surfaces all showed a reduced CA (Figure 2d, magenta). However, a significant decrease in CA change was observed when the initial contact angle was adjusted slightly above  $90^\circ$ . This indicates that the mesoporous films functionalized by spiropyran prevent water imbibition in this wetting range. The isomerization of spiropyran to its merocyanine isomer as a result of

light exposure thus causes a significant contact angle decrease of  $\approx 15^\circ$  since it takes place at a wetting transition from water exclusion to water imbibition, as described by Groten et al. for structured surfaces.<sup>[9c]</sup>

When increasing the amount of grafted APDMES, the trigger at the wetting transition can potentially be amplified. By adjusting the concentration in the reaction solution to 0.05 wt% and the reaction time to 4 h, the amount of spiropyran was increased. Figure 3a shows that CA changes of up to  $30^\circ$  were obtained. To the best of our knowledge, CA changes of that order of magnitude caused by spiropyran isomerization have not yet been observed for mesoporous thin films. Only adding, for example, metal ions, which promote the equilibrium of the isomerization to the merocyanine form, resulted in similar changes and only for randomly generated porosity and

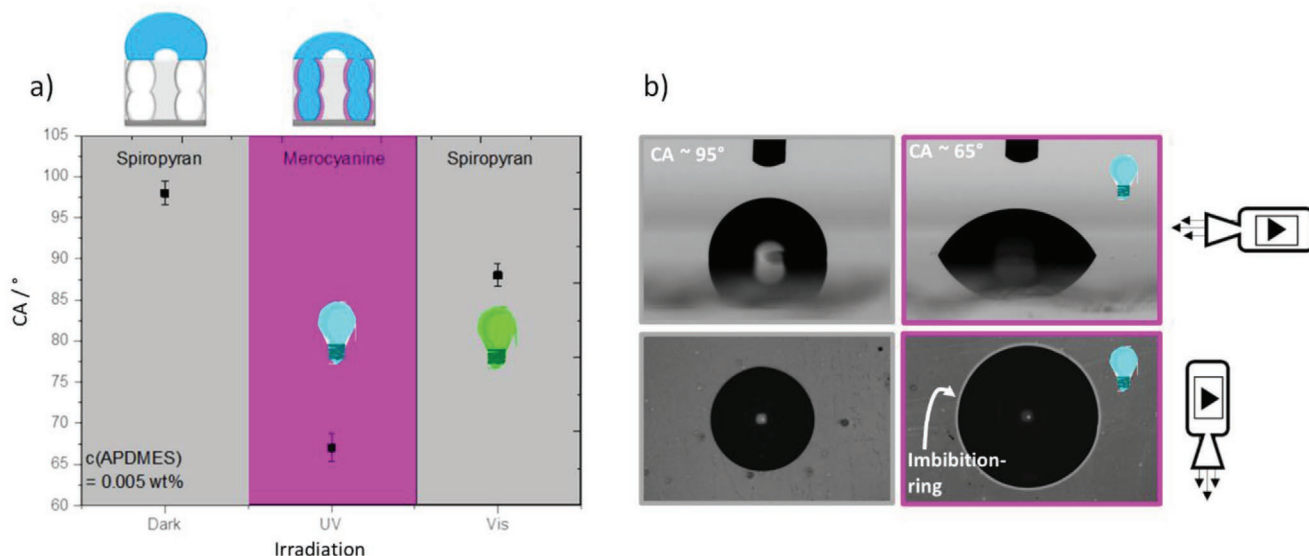


**Figure 3.** a) CA of mesoporous silica thin films after spiropyran esterification (gray) (post APDMES grafting with a 0.05 wt% solution) and subsequent UV-Light (magenta, irradiation time = 30 s) and visible light (Vis) irradiation (gray again, irradiation time = 120 s). b) Effect of photoisomerization to the merocyanine form on wettability, shown by imaging a droplet from the side as well as from the top. The top view reveals imbibition in the mesoporous film by showing a white ring around the droplet.

thickness.<sup>[20]</sup> In this work, the addition of  $M^{2+}$  ions did not cause a further decrease in CA upon UV irradiation (see Figure S6, Supporting Information). This supports the hypothesis that significant CA changes due to wetting transitions were observed. This was already achieved by the photoswitch, so that the further addition of metal cations had only minor and not necessarily macroscopically detectable consequences. To analyze the wetting transition and water imbibition in more detail, a top-view camera with integrated collimated coaxial illumination was used. Upon irradiation and thus merocyanine formation, the contact angle was reduced such that water imbibed into the mesoporous film. As the film thickness and pore size had nanoscale dimensions, evaporation strongly affected water imbibition. This resulted in the formation of an imbibition ring around the water droplet under equilibrium conditions (Figure 3b). For further explanation, please refer to previous work by our group<sup>[30]</sup> or by groups of Grosso or Berli, for example.<sup>[7a,b]</sup> Due to the imbibition of water into the mesopores, the refractive index of the material changed in such a way that the light was reflected and thus clearly demarcated in the form of the mentioned imbibition ring shown in white around the droplet (Figure 3b).

After the sample was exposed to visible (green) light, cleaned, and dried, the CA increased again to  $\approx 90^\circ$ , which was slightly lower than the initial CA. It should be noted that if the initial CA was not located close to a wetting transition, illumination and merocyanine formation did not cause major changes in the contact angle. If, for example, superhydrophobic silicon nanofilaments as used in Geyer et al.<sup>[31]</sup> were activated by plasma and then functionalized in accordance with Figure 2a, exposure to UV light showed hardly any effect, since the initial CA was too high to induce a wetting transition upon irradiation and merocyanine formation (see Figures S7 and S8, Supporting Information).

Furthermore, responsive molecules on the outer surface of the mesoporous films are necessary to induce noticeable

changes in wettability and water imbibition upon UV light exposure. By removing the amino groups on the outer surface using a  $CO_2$  plasma treatment according to Babu et al.,<sup>[32]</sup> prior to spiropyran grafting followed by the subsequent vapor deposition of perfluorooctyldimethylchlorosilane (PFODMCS) (according to a previous publication<sup>[26b]</sup>), a similar degree of hydrophobicity to that after normal spiropyran binding was achieved (see Figure S9, Supporting Information). Exposure to UV light did not show major CA changes for this functionalization strategy, which can be attributed to the absence of photoswitches on the outer mesoporous film surface (see Figure S10, Supporting Information).

### 2.1.2. Light-Gated Droplet Coalescence and Heat Absorption

Envisioning a surface that is able to manipulate, for example, to collect droplets while simultaneously filtering them, requires not only the control of water imbibition but also simultaneous control of droplet coalescence. The described photoresponsive contact angle change is able to induce light-triggered droplet coalescence while triggering water imbibition. To capture details of this process, such as the time dependence and the influence of the contact line shape, high-speed imaging from the top and side views was applied. To test for changes due to the fluid properties, experiments were performed using water and glycerol droplets, and both showed similar initial CAs (Figure 3; and Figure S11, Supporting Information). The spreading process took almost 4 s in the case of water (see also Videos S1 and S2, Supporting Information) and 20.5 s for glycerol. The time difference can be related to the higher viscosity of glycerin compared to water. This light-induced droplet spreading leads to a contact line movement of 0.3 mm for water and 0.15 mm for glycerin (corresponding to 11% and

12% of the drop radius, respectively), which was accompanied by a contact angle reduction of  $\approx 20^\circ$  for water and more than  $10^\circ$  for glycerin (see Figure S11, Supporting Information).

Not only can illumination by UV light induce droplet merging due to contact line movement, but it can also cause flows inside the drop due to light-triggered imbibition and heat uptake by the spiropyran chromophore (see also Videos S3 and S4, Supporting Information).

To visualize potential temperature changes and associated heat transport as well as a possible and filtering relevant fluid flow within the droplet upon UV irradiation, IR imaging and particle tracking (the setup is imaged in Figure S12, Supporting Information) were carried out.

The temperature-induced flows inside the droplet were visualized using particle tracking, which clearly demonstrated convection. Polystyrene particles, too large to enter the mesopores, were added to the water droplet and observed from the side. The convection cells were visible after 1.3 s of illumination as the particles started to move in an elliptical manner (see Video S4, Supporting Information) caused by water imbibition and light absorption, which caused an increase in surface temperature.

The temperature field for different irradiation times upon UV-light irradiation and thus merocyanine formation are depicted in Figure 4. UV-light irradiation induced a temperature increase of  $1.3^\circ\text{C}$  in the dry area and a temperature increase of  $0.9^\circ\text{C}$  under the center of the droplet after 2 s. After an irradiation time of 25 s, the temperature further increased by  $4.6^\circ\text{C}$  for the dry and  $4.1^\circ\text{C}$  for the wet area (Figure S13, Supporting Information). This temperature increase was caused by absorption of the applied UV light. As the substrate temperature increases faster than that of the water drops at the air–liquid interface, it can be assumed that this temperature difference

leads to Rayleigh–Bénard–Marangoni convection cells inside the drop.<sup>[33]</sup> There are two types of forces involved.

First, when the droplet is heated from below, the surface tension is reduced. This local variation in surface tension leads to Bénard–Marangoni convection cells.<sup>[24b]</sup> The surface tension decreases with increasing temperature. As a result, there is an induced flow from the region with lower surface tension to the region with higher surface tension. On the other hand, the viscosity resists this flow. Based on these two mechanisms, the nondimensional Marangoni number is defined to show whether the Bénard–Marangoni convection cells are formed.

$$Ma = \frac{\sigma_T \Delta T l}{\eta \kappa} \quad (1)$$

where  $\sigma_T = \partial\sigma/\partial T$  is the change in surface tension  $\sigma$  as a function of temperature  $T$ ;  $\Delta T$  is the temperature difference;  $l$  is the characteristic length, which is the height of the drop in this case;  $\eta$  is the dynamic viscosity of the fluid; and  $\kappa$  is the thermal diffusivity of the fluid.

If the Marangoni number is higher than a critical value, convection cells will form. If one excludes gravitational effects ( $g = 0$ ), the critical value of the Marangoni number for a thin film is  $Ma_c = 81$ .<sup>[24b]</sup> In the studied case, the temperature difference after 2 s is  $1.3$  for the dry part and  $0.9$  for the wet part. Then, we consider that the temperature difference between the top of the drop and the substrate is almost  $1.1^\circ\text{C}$ . Due to the physical characteristics of water, the Marangoni number is  $1700 \gg Ma_c$ .

Second, the temperature gradient in the drop also generates a density gradient of liquid in different regions. The resulting density difference can also induce convection, called Rayleigh–Bénard convection. The balance of the driving buoyant force and dissipative viscous drag in this case is given

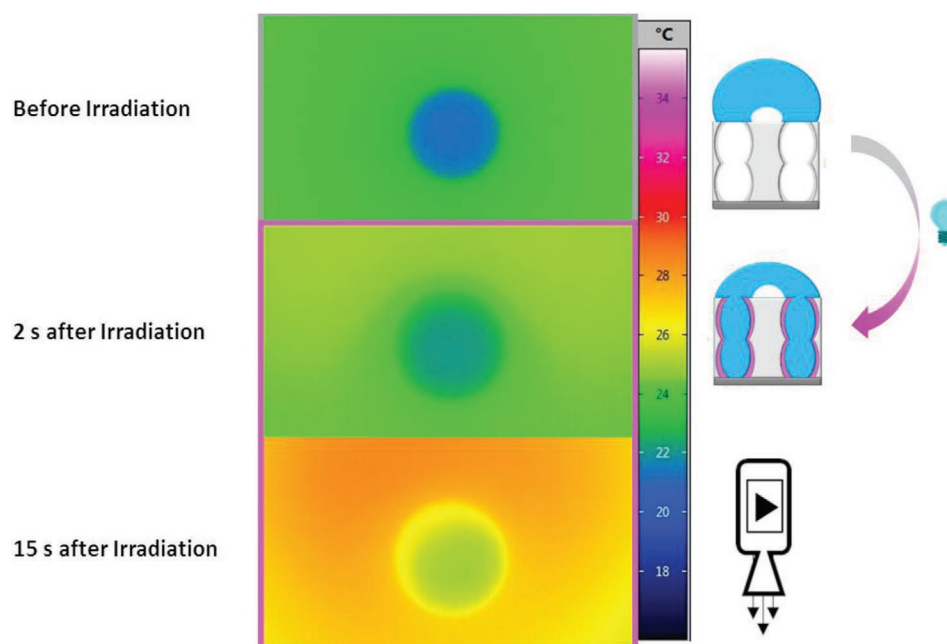


**Figure 4.** IR images of a  $9\ \mu\text{L}$  water drop on mesoporous silica thin films, showing the temperature rise due to UV light irradiation captured by IR cameras.

by the nondimensional Rayleigh number (Equation (2)). The onset of cells formation occurs when the Rayleigh number exceeds a critical value  $Ra_c$ .

$$Ra = \frac{g\beta\Delta Tl^3}{\nu\kappa} \quad (2)$$

where  $g$  is gravity acceleration;  $\beta$  denotes the coefficient of thermal volume expansion; and  $\nu$  is the kinematic viscosity.

The onset of convection for a liquid layer with a free upper surface (where the stress is zero) and a solid hot bottom wall is  $Ra_c \cong 1100$ .<sup>[33]</sup> In the studied case, the Rayleigh number is approximately 60. Although there are geometrical differences between the drop and liquid film, we can exclude buoyancy as the driving force for convection. The dominant driving force of the observed convection is gradients in surface tension.<sup>[34]</sup>

Finally, the use of light-induced contact line motion to cause droplet coalescence is demonstrated in **Figure 5**. The drops were placed close to each other, here, at a distance of approximately 0.3 mm. Light-induced drop spreading, contact, and drop merging were observed. Thus, we open the path for the light-induced control of droplet motion, which might find applications in water collection. In this context, Video S5, Supporting Information, also shows the coalescence of three droplets with the final droplet being formed in the downward direction of the tilted surface.

Consequently, when positioned at the transition from water exclusion to water infiltration, the molecular switch can change the macroscopic wetting properties of mesoporous silica thin films such that the applicative potential of the materials is increased immensely (droplet merging, controlled water flow, etc.). The spiropyran specifically changes not only the wetting properties of the material, resulting in simultaneous changes

in water imbibition and droplet coalescence but also the heat capacity and transport properties (see Figure 4). Therefore, Bénard–Marangoni flows, induced by heat absorption, can be used for filtering or to create a patterned functionalization inside a mesoporous matrix (see Figure S14, Supporting Information). The literature contains exciting examples that use the flows in ink droplets, for example, to create conducting surfaces by exploiting the “coffee ring” effect and deposit carbon nanotubes<sup>[25c]</sup> or silver nanoparticles in ring-shaped patterns.<sup>[35]</sup> In a similar manner, droplet deposition and evaporation of a solution could be used to create patterned surface functionalization in a porous system. Solvent infiltration accompanied by evaporation creates flows inside the droplet, which lead to an accumulation of molecules inside the porous network, as shown, for example, for a fluorescein-dyed water drop on a mesoporous silica thin film (see Figure S14, Supporting Information). Combining the water imbibition and simultaneous droplet coalescence control on mesoporous layers with a possible control of the Marangoni flow or suppression of the “coffee ring” effect<sup>[25b]</sup> by irradiation and molecule-specific heat absorption opens an interesting path for droplet filtering and structured molecule deposition in solid host materials.

### 3. Conclusion

In this work, we demonstrate a simultaneous photoswitching wetting transition that results in light-gated water imbibition with simultaneous switching of droplet coalescence on mesoporous silica thin films. Therefore, it is important to place the initial contact angle, determined by spiropyran molecules, close to the Cassie–Wenzel transition contact angle. Contact angle changes of  $\approx 30^\circ$  have been induced exclusively by light

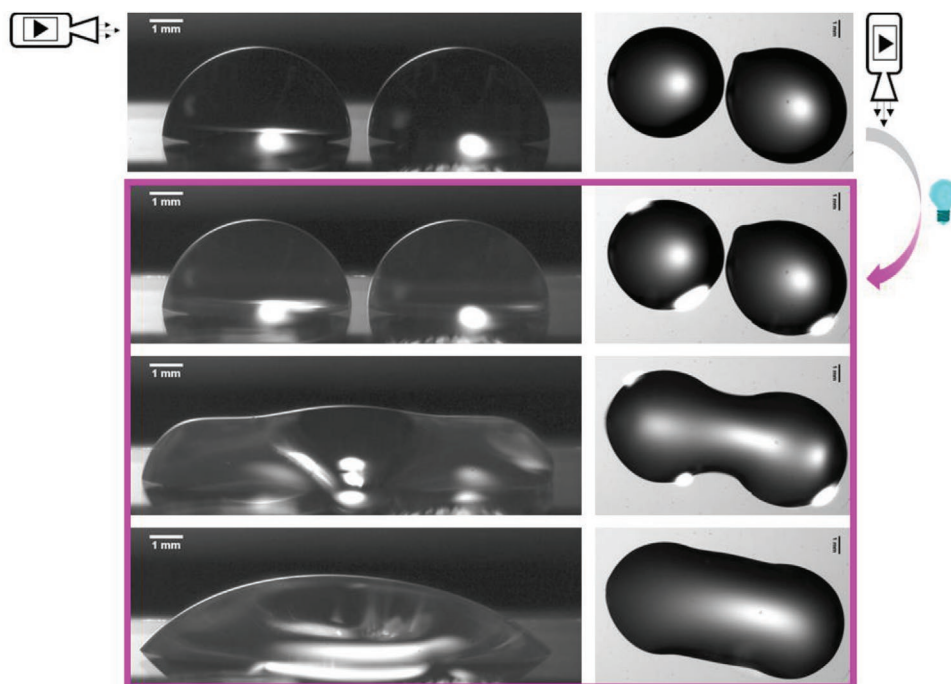


**Figure 5.** Droplet merging on mesoporous silica thin films caused by photoisomerization of spiropyran (top and sideview, scale bars = 1 mm).

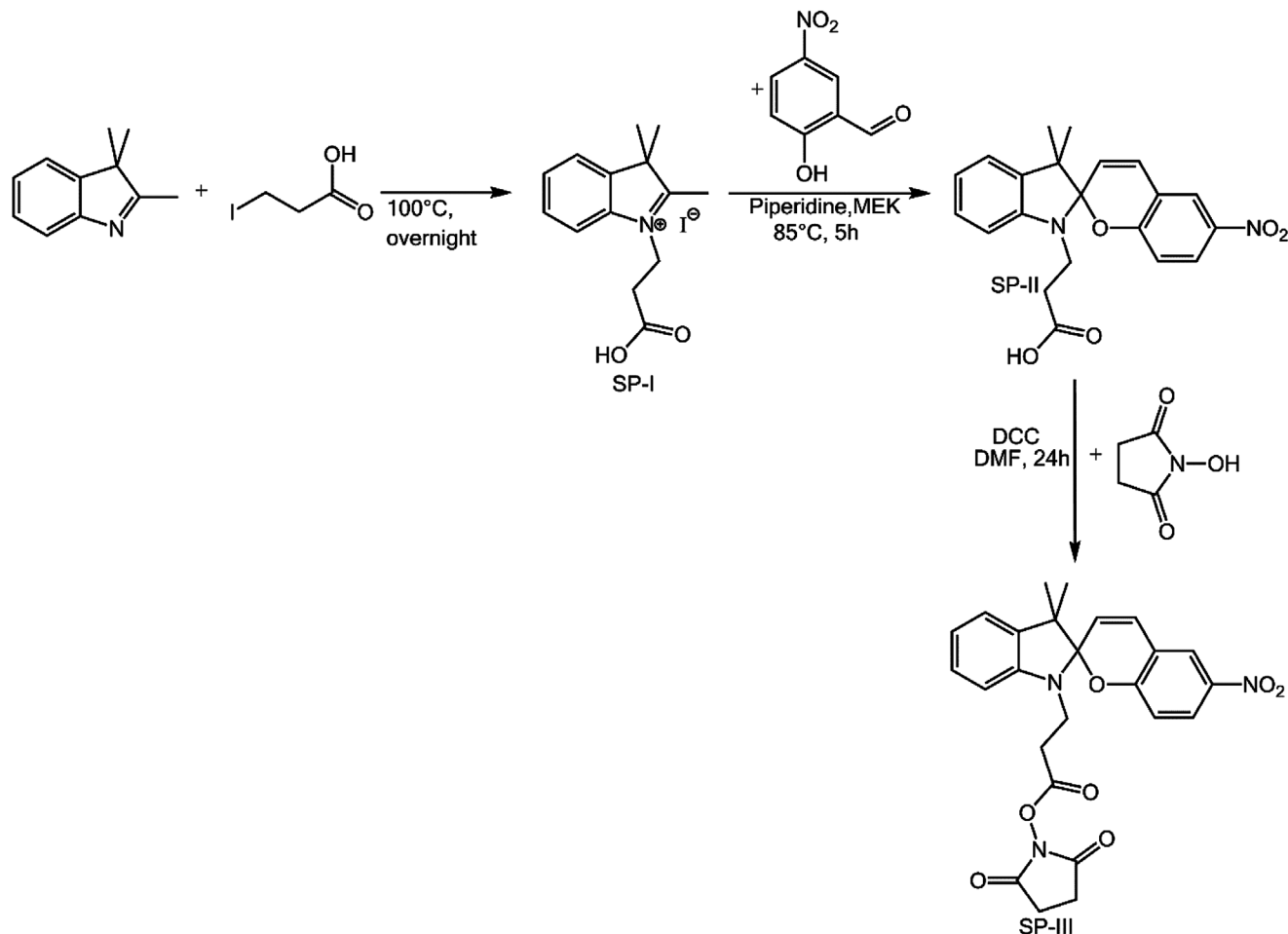
irradiation, resulting in a transition from water exclusion to water imbibition. Furthermore, it was shown that the irradiation of the spiropyran-modified mesopores caused an increase of 4–5 °C in the surface temperature. In combination with the light-triggered water imbibition, this leads to convection cells inside the droplet, which enables controlled molecule deposition or filtering in the mesoporous matrix. In general, the results shown are of the highest importance for all applications of mesoporous films or coatings that are based on solid–liquid interactions; for example, in nanofluidic devices, the light switch can be used to control the flow of ions or other small molecules. In particular, mesoporous films or coatings with externally controlled wetting transitions allow simultaneous droplet coalescence and filtering, presenting a further concept for future water management strategies.

#### 4. Experimental Section

**Reagents:** Pluronic F127, *N*-hydroxysuccinimide 98 % (NHS), anhydrous dimethylformamide (DMF) 99.8 %, 2,6-lutidine, 2,3,3-trimethylindolenine 98 %, and 3-aminopropyltriethoxysilane 99 % (APTES) were purchased from Sigma–Aldrich. Tetraethoxysilane (TEOS), 2-hydroxy-5-nitrobenzaldehyde and 3-iodopropionic acid were purchased from Alfa Aesar. Ethanol (absolute), anhydrous

2-butanone and anhydrous acetonitrile 99.8 % were purchased from Merck Millipore. 3-Aminopropyltriethoxysilane (APTES) and 3-aminopropyltrimethoxysilane 95 % (APTMS) were purchased from Acros Organics. 3-Aminopropyltrimethoxysilane (APDMES) and 3-aminopropyltrimethylmethoxysilane (APDMMS) were purchased from Fluorochem. Dry toluene (max. 0.005% water) was purchased from Applichem. All chemicals were used as received unless otherwise noted. **Synthesis of 1-(2-carboxyethyl)-2,3,3-trimethyl-3H-indol-1-ium-iodide (SP-I):** SP-I was synthesized according to a modified procedure from the literature.<sup>[36]</sup> Briefly, in a dry Schlenk flask, 5.4 g (25 mmol) of 3-iodopropionic acid was dried under vacuum for 30 min before 4 mL of dry 2-butanone and 4 g (25.3 mmol) of 2,3,3-trimethylindolenine were added in the counterflow of nitrogen. The reaction was heated to reflux and stirred under a nitrogen atmosphere overnight. The orange-red precipitate was dissolved in a minimum amount of water and extracted four times with dichloromethane. Subsequently, the united organic phase was extracted once with water. Under reduced pressure, the aqueous solution was concentrated until a yellow-orange salt is obtained (yield 98 %) (**Scheme 1**). The product was characterized by <sup>1</sup>H-NMR. <sup>1</sup>H NMR (300 MHz, DMSO-*d*<sub>6</sub>,  $\delta$ ) 8.02–7.94 (m, 1H, a), 7.87–7.80 (m, 1H, b), 7.62 (dd, *J* = 5.8, 3.1 Hz, 2H, c), 4.65 (t, *J* = 7.0 Hz, 2H, d), 2.98 (t, *J* = 7.0 Hz, 2H, e), 2.86 (s, 3H, f), 1.53 (s, 6H, g).

**Synthesis of 3-(3',3'-dimethyl-nitrospiro[chromene-2,2'-indoline]-1'-yl) Propionic Acid (SP-II):** SP-II was synthesized according to a modified procedure from the literature.<sup>[36]</sup> First, 20 mL of dry 2-butanone was added to a dry Schlenk flask containing 3.5 g (9.8 mmol) of SP-I. Afterward, 1 mL of freshly distilled piperidine and 1.68 g (10 mmol)



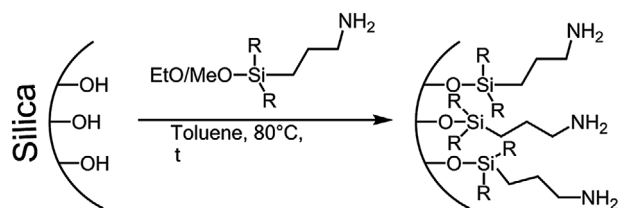
**Scheme 1.** Synthesis of SP-I, SP-II, and SP-III.



of 2-hydroxy-5-nitrosobenzaldehyde were added, whereupon a dark-violet solution was formed. The reaction mixture was refluxed for 5 h. Subsequently, the heat was removed, and the reaction mixture was stirred overnight under protection from light. Overnight, the reaction mixture changed color to red-brown and contained a yellow-brown precipitate. The solid was collected by filtration and washed with cold 2-butanone and methanol. A shiny yellow-green solid was obtained (yield 56 %) (Scheme 1). The product was characterized by  $^1\text{H-NMR}$ .  $^1\text{H NMR}$  (300 MHz, DMSO- $d_6$ ,  $\delta$ ) 11.38 (s, 1H, m), 7.40 (d,  $J = 2.8$  Hz, 1H, a), 7.18 (dd,  $J = 9.0, 2.8$  Hz, 1H, b), 6.39 (d,  $J = 10.4$  Hz, 1H, c), 6.35–6.27 (m, 2H, d), 6.08–5.93 (m, 2H, e+f), 5.88–5.81 (m, 1H, g), 5.18 (d,  $J = 10.4$  Hz, 1H, h), 2.76–2.54 (m, 2H, i), 1.86–1.56 (m, 2H, j), 0.37 (s, 3H, k), 0.26 (s, 3H, l).

**Synthesis of 2,5-dioxopyrrolidin-1-yl 3-(3',3'-dimethyl-6-nitrospiro[chromene-2,2'-indolenine]-1'-yl)Propanoate: (SP-III):** SP-III was synthesized according to a modified procedure from the literature.<sup>[37]</sup> In a dry Schlenk flask, 0.5 g (1.35 mmol) of SP-II, 0.27 g (1.28 mmol) of *N,N*-dicyclohexylcarbodiimide (DCC), and 0.16 g (1.4 mmol) of *N*-hydroxysuccinimide were dried under vacuum for at least 30 min. Afterward, the three solid components were dissolved in 13.5 mL of dry dimethylformamide (DMF), and the reaction mixture was stirred overnight at room temperature. The DMF was removed in vacuum, and the remaining violet solid residue was dissolved in 20 mL of ethyl acetate. The organic phase was extracted with 15 mL of a saturated, aqueous sodium bicarbonate solution and then washed three times with water. The organic layer was dried over magnesium sulfate and concentrated under vacuum, leaving behind a pale brown solid. The raw product was purified by recrystallization from ethyl acetate and petroleum ether (*n*-pentane). A yellow solid precipitated overnight (4 °C) as the final product and was obtained by filtration (yield 61 %) (Scheme 1). The product was characterized by  $^1\text{H-NMR}$ .  $^1\text{H NMR}$  (300 MHz, Chloroform- $d_3$ ,  $\delta$ ) 8.08–7.95 (m, 2H, a), 7.21 (dd,  $J = 7.7, 1.3$  Hz, 1H, b), 7.11 (ddd,  $J = 7.2, 1.3, 0.5$  Hz, 1H, c), 6.98–6.88 (m, 2H, d), 6.75 (dt,  $J = 8.3, 0.8$  Hz, 1H, e), 6.62 (d,  $J = 7.7$  Hz, 1H, f), 5.92 (d,  $J = 10.3$  Hz, 1H, g), 4.23–3.99 (EE), 3.76 (dt,  $J = 14.9, 7.4$  Hz, 1H, h), 3.56 (ddd,  $J = 15.0, 7.2, 5.6$  Hz, 1H, i), 3.04 (dt,  $J = 16.2, 7.3$  Hz, 1H, j), 2.83 (s, 4H, k), 2.04 (s, EE, DCU), 1.27 (s, 3H, l), 1.19 (s, 3H, m).

**Mesoporous Thin Film Preparation:** Mesoporous thin silica films were prepared by sol-gel chemistry using Pluronic F127 as a template in the presence of tetraethyl orthosilicate TEOS as a precursor. The precursor solution contained the following molar ratios: 1 TEOS: 0.0075 F127: 10 H<sub>2</sub>O: 40 ethanol: 0.28 HCl (37%). The solution was stirred overnight before being used for dipcoating to produce thin films with a withdrawal speed of 2 mm s<sup>-1</sup>. The thin films were deposited on glass, indium tin oxide (ITO, Delta Technologies) or silicon wafer (Si-Mat) substrates at a relative humidity (RH) of  $\approx 50\%$  and a temperature of  $\approx 23$  °C. Freshly deposited films were kept under these climate conditions for at least 1 h before being thermally treated. The films underwent two consecutive stabilization steps by being heated to 60 °C in 10 min and maintained this temperature for 1 h. Afterward, the temperature was increased to 130 °C in 10 min and again maintained for 1 h. Next, the temperature was increased to 350 °C at a rate of 1 °C min<sup>-1</sup> and maintained for 2 h



R = Alkyl, Alkoxy, OSi, OSiOR

**Scheme 2.** Grafting of different amino silanes (APTES, APDMMES, APDMES) to mesoporous silica.

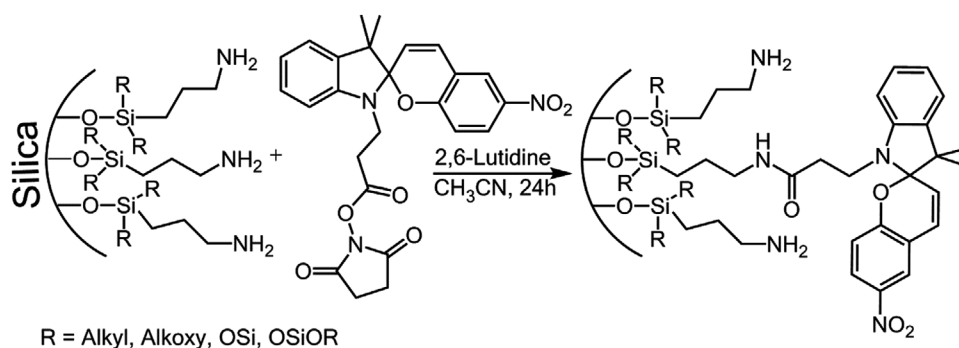
to burn out the organic template. Finally, the samples were rinsed with ethanol, producing films with pore diameters of 6–8 nm, thicknesses of  $\approx 130$ –250 nm and a porosity of  $\approx 50\%$  measured by ellipsometry.<sup>[38]</sup>

**Surface Grafting of Aminosilane:** The mesoporous thin films were immersed in a solution of wt%-aminosilane (APTES, APDMMES, APDMES) in dry toluene and stored in this solution for different periods of time at 80 °C (Scheme 2). Subsequently, the samples were rinsed with toluene and ethanol and extracted in ethanol.

**Grafting of SP-III to Silica Surface:** In a dry Schlenk flask, 30 mg of SP-III was dissolved in 30 mL of anhydrous acetonitrile. Afterward, four drops of freshly distilled 2,6-lutidine were added. The solution was used to overlay the amine-functionalized samples in a separate dry Schlenk tube. The samples were stored overnight in the solution with light excluded and under a nitrogen atmosphere (Scheme 3). Subsequently, the samples were rinsed and extracted in acetonitrile and stored in the dark until use.

**Ellipsometry:** Ellipsometry measurements were performed on reflecting silicon wafers (Si-Mat) using a Nanofilm Model EP3 imaging ellipsometer to determine the film thicknesses and refractive indices of the mesoporous thin films before and after functionalization. Therefore, one zone angle of incidence (AOI) variation measurements were captured between 38° and 68° in steps of 2° with a laser of 658 nm. The apparent film thicknesses and refractive indices were calculated from the measured ellipsometric angles  $\Psi$  and  $\Delta$ , using the EP4 analysis software supplied with the instrument. The measured data were fitted with a one-layer box model. The fitting range covered a film thickness from 100 to 250 nm and a refractive index range of 1 to 1.5. All films were measured at three identically marked positions before and after functionalization. Changes were calculated for each specific position followed by mean value and error determination. To determine the porosity from the refractive indices, the Bruggemann effective medium approximation was used. Standard ellipsometry measurements were performed at an RH of 15%.<sup>[39]</sup>

**UV-Vis Spectroscopy:** UV-vis and kinetic measurements of spirocyan and/or spirocyan-modified surfaces were performed by a Cary 60 UV-vis spectrometer (Agilent). The data were recorded by Agilent Cary WinUV-Software. All data were background corrected prior to each measurement.



R = Alkyl, Alkoxy, OSi, OSiOR

**Scheme 3.** Grafting of SP-III to amine-functionalized mesoporous silica.

**Contact Angle:** Contact angles (CA) were measured as deposited with an OCA 35 device by DataPhysics using the SCA 4.5.2 software and the sessile drop method under standard atmosphere ( $T = 23\text{ }^{\circ}\text{C}$ ,  $\text{RH} = 50\%$ ). A drop volume of  $2\text{ }\mu\text{L}$  was used, and the CA value was obtained by fitting the droplet shape using the approximation algorithm of the SCA software. The mean CA was measured for at least five droplets. The droplets were then removed from the sample, and after cleaning with ethanol (+ drying), the sample was exposed to light (see below for details) before the next measurements were performed.

**Irradiation of the Samples:** The surfaces were illuminated with a Lumatec lamp Model Superlite including different cutoff filters ( $\lambda_{\text{UV}} = 320\text{--}400\text{ nm}$ ,  $I = 11.8\text{ mW}\cdot\text{cm}^{-2}$  and  $\lambda_{\text{vis,green}} = 550\text{ nm}$ ,  $I = 11.8\text{ mW}\cdot\text{cm}^{-2}$ ). The samples were irradiated at a distance of  $3.0\text{ nm}$  and an angle of  $45^{\circ}$  to the sample, if not otherwise noted. To achieve the maximum amount of merocyanine, the samples were irradiated for at least  $30\text{ s}$  with UV light (determined by UV-vis measurements, see Figure S1a, Supporting Information). For backswitching, the samples were irradiated with visible, green light for at least  $120\text{ s}$  (determined by UV-vis measurements, see Figure S1b, Supporting Information).

**High Speed and IR Imaging System:** To capture the contact line and contact angle changes, the test section was observed from the top and side by a high-speed camera (Photron miniAX200 with a 2X F mount and a maximum 12X zoom lens from NAVITAR Co.). For homogenous illumination, an LED lamp (SCHOTT KL 2500 LED) along the diffuser sheet was employed. For particle tracking experiments, polystyrene particles (PS/Q-R-L2580 microparticles GmbH) were used. For the temperature field on the substrate, an IR camera (VarioCAM HD 600, InfraTec GmbH) was used.

## Supporting Information

Supporting Information is available from the Wiley Online Library or from the author.

## Acknowledgements

The authors kindly acknowledge the financial support by the German Research Foundation (DFG) within the Collaborative Research Centre 1194 "Interaction between Transport and Wetting Processes", Project-ID 265191195, subprojects C04, A02. In addition, the authors wish to thank Ulrike Kunz for TEM imaging, Florian Geyer (research group of Prof. D. Vollmer and Prof. H.-J. Butt, Max Planck Institute for Polymer Research, Mainz, Germany) for providing silicon nanofilaments and Prof. M. Biesalski for access to analytic equipment and infrastructure.

Open access funding enabled and organized by Projekt DEAL.

## Conflict of Interest

The authors declare no conflict of interest.

## Data Availability Statement

Research data are not shared.

## Keywords

mesoporous silica thin films, spiropyran, wetting properties, wetting transition

Received: March 17, 2021  
Published online: May 24, 2021

- [1] a) S. Karan, S. Samitsu, X. Peng, K. Kurashima, I. Ichinose, *Science* **2012**, *335*, 444; b) J. Liu, N. Wang, L.-J. Yu, A. Karton, W. Li, W. Zhang, F. Guo, L. Hou, Q. Cheng, L. Jiang, *Nat. Commun.* **2017**, *8*, 1.
- [2] a) S. Zhang, B. Zhang, H. Liang, Y. Liu, Y. Qiao, Y. Qin, *Angew. Chem., Int. Ed.* **2018**, *57*, 1091; b) E. Castillejos, P. J. Debouttière, L. Roiban, A. Solhy, V. Martinez, Y. Kihn, O. Ersen, K. Philippot, B. Chaudret, P. Serp, *Angew. Chem., Int. Ed.* **2009**, *48*, 2529.
- [3] a) X. Zhang, H. Liu, L. Jiang, *Adv. Mater.* **2019**, *31*, 1804508; b) D. Lin, Y. Liu, Y. Cui, *Nat. Nanotechnol.* **2017**, *12*, 194; c) J. Chen, D. Wu, E. Walter, M. Engelhard, P. Bhattacharya, H. Pan, Y. Shao, F. Gao, J. Xiao, J. Liu, *Nano Energy* **2015**, *13*, 267; d) D. Lin, Y. Liu, Z. Liang, H.-W. Lee, J. Sun, H. Wang, K. Yan, J. Xie, Y. Cui, *Nat. Nanotechnol.* **2016**, *11*, 626.
- [4] C. J. Brinker, Y. Lu, A. Sellinger, H. Fan, *Adv. Mater.* **1999**, *11*, 579.
- [5] C. Sanchez, C. Boissiere, D. Grosso, C. Laberty, L. Nicole, *Chem. Mater.* **2008**, *20*, 682.
- [6] a) M. Tagliazucchi, I. Szleifer, *Mater. Today* **2015**, *18*, 131; b) L. Nicole, C. Boissiere, D. Grosso, A. Quach, C. Sanchez, *J. Mater. Chem.* **2005**, *15*, 3598; c) D. Grosso, *J. Mater. Chem.* **2011**, *21*, 17033; d) S. Alberti, G. J. Soler-Illia, O. Azzaroni, *Chem. Commun.* **2015**, *51*, 6050; e) X. Hou, F. Yang, L. Li, Y. Song, L. Jiang, D. Zhu, *J. Am. Chem. Soc.* **2010**, *132*, 11736.
- [7] a) D. R. Ceratti, M. Faustini, C. Sinturel, M. Vayer, V. Dahirol, M. Jardat, D. Grosso, *Nanoscale* **2015**, *7*, 5371; b) M. Mercuri, K. Pierpauli, M. G. Bellino, C. L. Berli, *Langmuir* **2017**, *33*, 152; c) R. Urteaga, M. Mercuri, R. Gimenez, M. G. Bellino, C. L. Berli, *J. Colloid Interface Sci.* **2019**, *537*, 407.
- [8] a) H.-J. Butt, C. Semperebon, P. Papadopoulos, D. Vollmer, M. Brinkmann, M. Ciccotti, *Soft Matter* **2013**, *9*, 418; b) B. Bhushan, *Langmuir* **2012**, *28*, 1698; c) J. Lv, Y. Song, L. Jiang, J. Wang, *ACS Nano* **2014**, *8*, 3152.
- [9] a) Z. Chu, S. Seeger, *Chem. Soc. Rev.* **2014**, *43*, 2784; b) B. Xin, J. Hao, *Chem. Soc. Rev.* **2010**, *39*, 769; c) J. Groten, C. Bunte, J. r. Rühle, *Langmuir* **2012**, *28*, 15038.
- [10] X. Yao, Y. Hu, A. Grinthal, T.-S. Wong, L. Mahadevan, J. Aizenberg, *Nat. Mater.* **2013**, *12*, 529.
- [11] a) S. Karpitschka, H. Riegler, *J. Fluid Mech.* **2014**, *743*, R1; b) P. Rostami, B. B. Straub, G. n. K. Auernhammer, *Langmuir* **2019**, *36*, 28; c) I. V. Roisman, C. Planchette, E. Lorenceau, G. Brenn, *J. Fluid Mech.* **2012**, *690*, 512.
- [12] a) B.-E. Pinchasik, M. Kappl, H.-J. r. Butt, *ACS Nano* **2016**, *10*, 10627; b) G. Zhao, G. Zou, W. Wang, R. Geng, X. Yan, Z. He, L. Liu, X. Zhou, J. Lv, J. Wang, *ACS Appl. Mater. Interfaces* **2020**, *12*, 7805.
- [13] Y. Cheng, Y. Liu, X. Ye, M. Liu, B. Du, Y. Jin, R. Wen, Z. Lan, Z. Wang, X. Ma, *Chem. Eng. J.* **2020**, *405*, 126901.
- [14] G. Zhao, G. Zou, W. Wang, R. Geng, X. Yan, Z. He, L. Liu, X. Zhou, J. Lv, J. Wang, *Soft Matter* **2020**, *16*, 4462.
- [15] a) Y. Hou, Y. Shang, M. Yu, C. Feng, H. Yu, S. Yao, *ACS Nano* **2018**, *12*, 11022; b) X. Yan, L. Zhang, S. Sett, L. Feng, C. Zhao, Z. Huang, H. Vahabi, A. K. Kota, F. Chen, N. Miljkovic, *ACS Nano* **2019**, *13*, 1309; c) X. Yan, F. Chen, X. Zhang, Y. Qin, C. Zhao, S. Sett, H. Cha, M. J. Hoque, F. Zhao, Z. Huang, *Adv. Mater. Interfaces* **2020**, *7*, 2000475.
- [16] a) K. Ichimura, S.-K. Oh, M. Nakagawa, *Science* **2000**, *288*, 1624; b) E. Rossegger, D. Hennen, T. Griesser, I. Roppolo, S. Schlögl, *Polym. Chem.* **2019**, *10*, 1882; c) Y. Liu, L. Mu, B. Liu, J. Kong, *Chem. - Eur. J.* **2005**, *11*, 2622.
- [17] a) D.-M. Drotlef, P. Blümler, P. Papadopoulos, A. n. del Campo, *ACS Appl. Mater. Interfaces* **2014**, *6*, 8702; b) M. Macias-Montero, A. Borrás, R. Alvarez, A. R. Gonzalez-Elipe, *Langmuir* **2012**, *28*, 15047.
- [18] R. Klajn, *Chem. Soc. Rev.* **2014**, *43*, 148.
- [19] a) M. Bletz, U. Pfeifer-Fukumura, U. Kolb, W. Baumann, *J. Phys. Chem. A* **2002**, *106*, 2232; b) M. Levitus, G. Glasser, D. Neher, P. F. Aramendía, *Chem. Phys. Lett.* **1997**, *277*, 118; c) Q. Shen, Y. Cao, S. Liu, M. L. Steigerwald, X. Guo, *J. Phys. Chem. C* **2009**, *113*, 10807.

- [20] D. Dattilo, L. Armelao, G. Fois, G. Mistura, M. Maggini, *Langmuir* **2007**, *23*, 12945.
- [21] R. Rosario, D. Gust, A. A. Garcia, M. Hayes, J. Taraci, T. Clement, J. Dailey, S. Picraux, *J. Phys. Chem. B* **2004**, *108*, 12640.
- [22] S. Samanta, J. Locklin, *Langmuir* **2008**, *24*, 9558.
- [23] S. Herminghaus, *Phys. Rev. Lett.* **2012**, *109*, 236102.
- [24] a) J. Maroto, V. Pérez-Munuzuri, M. Romero-Cano, *Eur. J. Phys.* **2007**, *28*, 311; b) J. Pearson, *J. Fluid Mech.* **1958**, *4*, 489; c) R. E. Sakhy, K. El Omari, Y. Le Guer, S. Blancher, *Int. J. Therm. Sci.* **2014**, *86*, 198.
- [25] a) M. Layani, M. Gruchko, O. Milo, I. Balberg, D. Azulay, S. Magdassi, *ACS Nano* **2009**, *3*, 3537; b) P. J. Yunker, T. Still, M. A. Lohr, A. G. Yodh, *Nature* **2011**, *476*, 308; c) A. Shimon, S. Azoubel, S. Magdassi, *Nanoscale* **2014**, *6*, 11084.
- [26] a) A. Brunsen, A. Calvo, F. J. Williams, G. J. Soler-Illia, O. Azzaroni, *Langmuir* **2011**, *27*, 4328; b) A. Khalil, M. Zimmermann, A. K. Bell, U. Kunz, S. Hardt, H.-J. Kleebe, R. W. Stark, P. Stephan, A. Andrieu-Brunsen, *J. Colloid Interface Sci.* **2020**, *560*, 369.
- [27] F. Krohm, J. Kind, R. Savka, M. A. Janßen, D. Herold, H. Plenio, C. Thiele, A. Andrieu-Brunsen, *J. Mater. Chem. C* **2016**, *4*, 4067.
- [28] Y. Okabe, M. Ogawa, *RSC Adv.* **2015**, *5*, 101789.
- [29] a) H. H. Kyaw, S. H. Al-Harhi, A. Sellai, J. Dutta, *Beilstein J. Nanotechnol.* **2015**, *6*, 2345; b) E. Asenath Smith, W. Chen, *Langmuir* **2008**, *24*, 12405.
- [30] A. Khalil, F. Schäfer, N. Postulka, M. Stanzel, M. Biesalski, A. Andrieu-Brunsen, *Nanoscale* **2020**, *12*, 24228.
- [31] F. Geyer, M. D'Acunzi, C. Y. Yang, M. Müller, P. Baumli, A. Kaltbeitzel, V. Mailänder, N. Encinas, D. Vollmer, H. J. Butt, *Adv. Mater.* **2019**, *31*, 1801324.
- [32] D. J. Babu, S. Yadav, T. Heinlein, G. Cherkashinin, J. r. J. Schneider, *J. Phys. Chem. C* **2014**, *118*, 12028.
- [33] S. Chandrasekhar, *Hydrodynamic and Hydromagnetic Stability*, Courier Corporation **2013**.
- [34] a) S. Manukyan, H. M. Sauer, I. V. Roisman, K. A. Baldwin, D. J. Fairhurst, H. Liang, J. Venzmer, C. Tropea, *J. Colloid Interface Sci.* **2013**, *395*, 287; b) A. Marin, S. Karpitschka, D. Noguera-Marín, M. A. Cabrerizo-Vílchez, M. Rossi, C. J. Kähler, M. A. R. Valverde, *Phys. Rev. Fluids* **2019**, *4*, 041601; c) Y. Ren, R. Xue, W. Liu, Y. Tao, F. Bao, *J. Micromech. Microeng.* **2020**, *30*, 085007; d) R. Xue, W. Liu, T. Jiang, C. Song, H. Jiang, Y. Ren, *Adv. Mater. Interfaces* **2020**, *7*, 2000345.
- [35] S. Magdassi, M. Grouchko, D. Toker, A. Kamyshny, I. Balberg, O. Millo, *Langmuir* **2005**, *21*, 10264.
- [36] A. Fissi, O. Pieroni, G. Ruggeri, F. Ciardelli, *Macromolecules* **1995**, *28*, 302.
- [37] P. Zhang, J. Meng, X. Li, Y. Wang, T. Matsuura, *J. Heterocycl. Chem.* **2002**, *39*, 179.
- [38] C. Boissiere, D. Grosso, S. Lepoutre, L. Nicole, A. B. Bruneau, C. Sanchez, *Langmuir* **2005**, *21*, 12362.
- [39] J. E. Spanier, I. P. Herman, *Phys. Rev. B* **2000**, *61*, 10437.